

Rare Earth Glass Reference Materials for Near Infrared Spectrometry:
Sources of X-Axis Location Variability

David L. Duewer*, Steven J. Choquette, and Lindsey O'Neal

Analytical Chemistry Division, Chemical Science and Technology Laboratory,
National Institute of Standards and Technology, Gaithersburg, MD 20899-8394

James J. Filliben

Statistical Engineering Division, Information Technology Laboratory,
National Institute of Standards and Technology, Gaithersburg, MD 20899-8980

Intended for the
Chemometrics in Analytical Chemistry 2002
Special Issue

* Corresponding Author: David Lee Duewer
NIST
100 Bureau Drive, Stop 8394
Gaithersburg, MD 20899-8394
USA
Tel: 301-975-3935
Fax: 301-977-0685
Eml: david.duewer@nist.gov

ABSTRACT

The National Institute of Standards and Technology recently introduced two optical filter standards for wavelength/wavenumber calibration of near-infrared (NIR) spectrometers. Standard Reference Materials (SRMs) 2035 and 2065 were fabricated in lots of ≈ 100 units each from separate melts of nominally identical rare-earth glass. Since individual filter certification is extremely time-consuming and thus costly, economic production of these SRMs required the ability to batch certify band locations. Given the specification that the combined uncertainty for the location of the bands in a given filter should be $\leq 0.2 \text{ cm}^{-1}$, rigorous evaluation of material heterogeneity was required to demonstrate the adequacy of batch certification for these materials. Among-filter variation in measured band locations convolves any influence of material heterogeneity with that of environmental, procedural, and instrumental artifacts. While univariate analysis of variance established band-specific heterogeneity upper bounds, it did not provide quantitative descriptions of the other possible sources for the observed measurement variability. Principal components analysis enabled both the identification and isolation of the most important NIR band location variances among the SRM 2065 filters. After correction for these variance sources, the upper bound on the material heterogeneity was determined to be 0.03 cm^{-1} for all bands. Since this is a small part of the measurement uncertainty, we conclude that batch analysis provides an acceptable certification approach for these and similarly fabricated rare-earth glass reference materials.

INDEXING TERMS

Material Homogeneity
Optical filters
Principal Components Analysis (PCA)
Spectrometer x-axis calibration
Temperature correction

INTRODUCTION

The National Institute of Standards and Technology (NIST) recently introduced two rare-earth glass optical filter Standard Reference Material[®]s (SRM[®]s) suitable for the verification and calibration of the x-axis (as wavenumber, cm^{-1} , or wavelength, nm) of near infrared (NIR) spectrometers operating in transmittance mode. SRM 2035 Near Infrared Transmission Wavelength Standard from $10\,300\text{ cm}^{-1}$ to 5130 cm^{-1} was issued in early 1999 [1, 2]. SRM 2065 UV-Visible, Near-Infrared Transmission Wavelength/Vacuum Wavenumber Standard was issued in early 2002 [3]. The x-axis locations of the spectral features in both SRMs are batch-certified; that is, the properties of interest in every unit of the given SRM have been determined from the analysis of a statistically valid subset of the units and are certified to be identical within specified limits.

Successful batch certification depends upon adequate material homogeneity; that is, unit-to-unit variation in the certified properties due to differences in material composition must be an acceptably small part of the total uncertainty. All SRM 2035 and SRM 2065 filters were ground from separately ordered single-crucible glass melts, with each melt supplied in the form of a single glass slab. While both slabs were of excellent optical quality, this visual homogeneity does not exclude the possibility of localized within-slab differences that could affect the NIR properties of interest. While no statistically significant among-filter differences were observed during the SRM 2035 characterization and certification experiments, resources did not permit full assessment of the sources of the acceptably small measurement variability observed.

Guided by our experience with SRM 2035, an experimental design was developed to identify subtle among-filter differences for the nominally identical glass of SRM 2065. Acquisition of replicate spectra for essentially all SRM 2065 filters and a single SRM 2035 control filter combined with simple multivariate data analysis techniques enabled the identification, isolation, and quantitative assessment of the environmental and instrumental

factors responsible for the observed band-location variability. We present here the experimental and data analytic techniques used to demonstrate that batch certification of NIR spectral feature locations in single melts of rare-earth glass is indeed appropriate.

MATERIALS, METHODS, AND MEASUREMENTS

SRM 2065

The rare-earth glass used for SRM 2065 was purchased from Schott Glass Technologies (Dureya, PA, USA); compositional details are presented elsewhere [2]. Approximately 100 filter blanks were ground and polished at NIST to a diameter of 25.4 mm and thickness of 1.5 ± 0.1 mm. These blanks were arbitrarily assigned labels from 201 to 297. There is no known relationship between the blank's label and its original glass block location or the order in which it was ground. Eighty-five of these filters were available at the time these studies were performed.

Spectrophotometer

All spectra used for homogeneity assessment were acquired with a Bruker IFS66 Fourier Transform (FT) spectrometer (Bruker Optics Inc., Billerica, MA, USA). This spectrometer is equipped with a helium-neon (HeNe) laser, a tungsten white-light source, a silicon-coated CaF_2 beamsplitter, and a liquid-nitrogen-cooled InSb detector. All spectra were acquired in a NIST-constructed external sample chamber designed to allow use of a six-filter autosampler and enhance control of the sample environment. A recirculating water bath and several meters of tubing are used to control the temperature of the external sample chamber; the temperature of the bath is controlled to 25.0 ± 0.5 °C. The instrument and external sample chamber are purged with dry nitrogen. The observed long-term system precision standard deviation, determined from analysis of water vapor spectral bands, is 0.03 cm^{-1} . The spectrophotometer calibration and qualification protocols are detailed elsewhere [2 - 4].

Spectra

Each FT-NIR spectrum is the ratio between two single-channel sets of data, I/I_0 , where I represents signal through the sample and I_0 signal through just the purge-gas. The two sets are acquired sequentially, both as 256 co-added, double-sided, forward and backward scans of

the interferometer at 4.0 cm^{-1} nominal resolution. The interferometer scan speed of 20 kHz is optimized for the detector. An internal beam aperture of 1.0 mm is used to ensure adequate collimation of the source. To ensure linear response of the liquid-nitrogen-cooled InSb detector, a wire attenuation screen is placed in the path of the beam before the sample; this limits the center burst amplitude to half of the full-scale response. The resulting single-channel spectral amplitudes are no more than 0.5% of the peak response in the 2000 cm^{-1} and below cutoff region of the detector. Mertz phase correction and a Blackman-Harris three-term apodization function are applied to all raw interferograms. Each interferogram is zero-filled by a factor of 4, yielding a data interval of 0.97 cm^{-1} . The absorbance versus wavenumber spectra are calculated from these data using Opus v3.1 software (Bruker Optics Inc., Billerica, MA, USA).

Experimental Designs

Primary Study. Replicate spectra for all 85 SRM 2065 filters were acquired during a period of continuous spectrophotometer operation from June 11 through June 23, 1999. Filters were measured in groups of six, with the SRM 2035 control filter in autosampler wheel position #0 and pre-selected randomized groups of five SRM 2065 filters in positions #1 through #5. The control filter was not manipulated during the course of this experiment. Spectra were acquired for the six filters in filter wheel position sequence, one spectrum per filter during each of six filter wheel rotations plus return to position #0. The entire set of 37 spectra (six replicate spectra of the five SRM 2065 filters and seven replicate spectra of the control filter) is termed a “run”. Each run required approximately 3.5 h.

The following exceptions to the design occurred: (1) SRM 2065 #206 was included in runs #1 and #6, providing 12 replicate spectra for this filter. (2) The final six spectra of run #13 were invalidated by the loss of liquid-nitrogen cooling to the InSb detector, thus there are only five replicate spectra for SRM 2065 #281 through #285 and only six control replicates for this run. (3) Only four SRM 2065 filters were included in run #16. (4) Only two SRM 2065 filters

were included in the final run #18. The entire homogeneity experiment thus required 18 runs and acquired 511 SRM 2065 spectra (85 different filters) and 125 control spectra (one filter). Spectra were acquired on nine different days during the two-week period, typically two runs were accomplished in a given day, but there were two “long” days of three runs and two “short” days of one run.

The spectrophotometer was calibrated prior to measuring the entire series of filters. The x-axis calibration was qualified daily. Temperature readings at the autosampler were recorded at the beginning and end of each run.

Follow-Up Study. Approximately nine months after acquisition of the primary homogeneity data, new spectra were acquired for ten selected SRM 2065 filters. The same instrumental parameters were used as described above. There were no between-study modifications of spectrophotometer hardware or software. The only conscious procedural change between studies was adoption of a somewhat longer (≈ 30 min) initial purge of the external sample box before beginning spectral acquisition.

The filters of the follow-up study were selected to represent the “extreme endpoints” of potential among-filter band location heterogeneity (factor f''_2 , described below), based upon analysis of the primary data. Under the constraint of using only one filter from any of the original study’s groupings, five filters were identified from the “extremely negative” and five from the “extremely positive” ends of the putative heterogeneity distribution. These ten filters were studied as two sets of five: one set of three “negative” and two “positive” filters and for the other set the reverse. Five runs of 37 spectra were collected in a period of two sequential days, two runs of one set and three of the other, for a total of 35 new control filter and 150 new SRM 2065 spectra.

Data Analysis

The characteristic x-axis location of the j^{th} absorption band in the i^{th} spectrum is estimated throughout as the 10% peak-fraction “center-of-gravity” or centroid, b_{ij} [5]. The b_{ij} estimates for all filter spectra were calculated using the algorithm specified in ASTM E1421-99 [6] implemented as an array basic macro in Grams_32 (Thermo Galactic Industries, Salem, NH, USA). All analysis of x-axis location data was performed using Microsoft Excel[®] 97 (Microsoft Corp, Redman, WA, USA) and the Bristol Chemometrics Group’s (School of Chemistry, University of Bristol, Bristol, UK) *free* Multivariate Analysis add-in [7]. The Excel[®]-environment results were confirmed by comparison to for-purpose MATLAB[®] (The MathWorks Inc., Natick, MA, USA) calculations.

RESULTS AND DISCUSSION

Absorption Bands

SRM 2035 and 2065 provide seven absorption bands, denoted “B₁” through “B₇”, between 5130 cm⁻¹ and 10300 cm⁻¹ of suitable intensity and shape for x-axis location certification. Figure 1 presents a representative absorbance spectrum of these materials and of the purge gas reference I₀. Bands B₁ and B₅ are holmium features, B₂, B₃, B₄, and B₆ are from samarium, and B₇ is from ytterbium. The lower segment of Figure 2 details the “top” 10% peak-fraction of the seven bands [5]. All of the bands are quite smooth and nearly symmetrical within this spectral window. The number of 4 cm⁻¹ resolution data within this window range from 26 (25 cm⁻¹) for B₇ to 128 (125 cm⁻¹) for B₆.

The purge gas-reference I₀ spectrum is a composite of the tungsten source emissivity, beamsplitter transmission, InSb detector response, and any absorption lines from gases in the instrument and external sample chamber. The upper segment of Figure 2 details I₀ spectral variability within each of the 10%-fraction windows, represented as the residual standard deviation of each relevant spectral channel of a representative group of normalized spectra. The multiple peaks in the B₁, B₂, and especially B₃ windows correspond to water vapor vibration-rotational lines [8]. The single lines in the B₅ and B₆ windows correspond with HeNe plasma emission lines [9].

Univariate Analysis

Table 1 summarizes results of the single-factor analysis of variance (ANOVA) of replicate b_{ij} measurements, with filter-identity used as the categorical variable [10]. To facilitate interpretation, the components of variance are represented in standard deviation form: within-filter (s_{within}), among-filter (s_{among}), and combined (s_{comb}). While s_{comb} is comfortably less than 0.1 cm⁻¹ for all bands except B₃, the among-filter / within-filter variance ratio (F) for these bands is larger than expected under the null hypothesis of zero true band-location differences.

The b_{i3} are more variable than those of the other bands. Further, s_{within} is larger than s_{among} only for B₃. This suggests that the b_{i3} are affected much differently and/or much more strongly by external factors than are the other band locations. This is compatible with the patterns of I_0 variability displayed in Figure 2.

For the other six bands, the SRM 2065 s_{comb} are quite similar to the control filter's s_{within} (for a single filter, there is no among-filter variability). This suggests the observed variabilities arise from properties of the measurement process rather than of the filters. More complete ANOVA models suggest that the variabilities are functions of procedural variables such as: sample filter wheel position (Position), filter measurement sequence (Filter), run sequence (Run), spectral acquisition sequence within run (Sequence), and replicate spectrum sequence within run (Duplicate). The s_{among} listed in Table 1 therefore represents an upper bound on any material heterogeneity effect.

None of the available procedural variables directly estimate the influence of any environmental or instrumental factor. While the temperature and gas-composition environment of the instrument and sample box are controlled via passive convective heating/cooling and purge-gas flow, neither are actively regulated and both may change slowly with time. (Indeed, the temperature measured near the filter wheel generally increased by about 0.5 °C over the course of a given run.) Likewise, neither the input nor the output power of the tungsten lamp and HeNe laser are actively regulated or monitored. As none of these factors were quantitatively evaluated during spectrum acquisition, the magnitude of their influence (if any) on band location is not directly determinable.

Multivariate Analysis

Principal components analysis (PCA) is a well-established method for linearly projecting a data matrix of mutually dependent (correlated) variables describing a set of objects onto a set of independent (uncorrelated) principal components (PCs) [11-13]. Typically, the data structure

chosen for representation is either the correlation or the mean-centered variance-covariance matrix. There are different mathematical formulations, definitions, and terms used to accomplish and describe the PCA process and results. All the various flavors of PCA generally provide – or can be further processed to provide – the same final information. In general, we follow Brereton's notation and terminology [11, 14].

The projected PCs retain all of the information about the objects provided by the original variables but in an isolated, concentrated, and often more interpretable form. They are typically ordered by decreasing importance for the representation of the selected data structure. One-at-a-time examination of the PCs can sometimes display otherwise hidden relationships among the objects. Insight into physically meaningful relationships among the original measurements can be gained from evaluating the factor loadings, the coefficients which project the original variables onto the PCs, and of the resulting projections or factor scores, f_{ik} .

PCA of Mean-Centered Data. Table 2 presents summary PCA results for the three most informative PCs for explaining the mean-centered variance-covariance structure of the b_{ij} measurements; i.e., the three PCs that account for the largest percentage of measurement variability. To facilitate interpretation, the contribution of each of the bands to the variability of each of the PCs is presented in standard deviation form. The variability of each band, s_b , is presented in the right-most column; the variability of each factor, s_f , is presented in the bottom row. The grand total variability over all the bands is identical to the grand total variability of the PCs – as it should be if the two representations are information-identical.

The first factor, f_1 , represents the dominant direction of variation in the original data. The f_{i1} are highly and positively correlated with the b_{ij} of all bands, suggesting a physical cause that affects all bands in a similar manner. Figure 3 displays the f_{i1} as functions of the various procedural variables. The large separation between most of the high magnitude 25% of the f_{i1} and the remainder of the scores reflects the differences between the spectra of the single SRM

2035 control and the 85 SRM 2065 filters. The \mathbf{f}_1 loadings are almost perfectly correlated with the difference between the SRM 2065 and SRM 2035 mean band locations (Table 1, $\Delta_{2065-2035}$). Factor \mathbf{f}_1 thus represents the differences in band location between the two SRM filter types. While trivial, confirmation of this “known heterogeneity” establishes the utility of the approach. More importantly, isolation of these between-material differences into a single PC facilitates evaluation of the residual variations captured in the smaller PCs by enabling direct comparison among all filters of a given Run.

PCA of SRM-Centered Data. The between-SRM heterogeneity is easily eliminated by centering the b_{ij} for the SRM 2035 and 2065 filters on their individual means rather than the global data mean. Table 3 presents summary PCA results for the three most informative PCs for this SRM-centered data, denoted as \mathbf{f}'_1 , \mathbf{f}'_2 , and \mathbf{f}'_3 to distinguish them from the globally-centered PCs.

The SRM-centered standard deviation for each band, s'_b , agrees well with the s_{comb} for SRM 2065 filters and the s_{within} for the SRM 2035 control filter (Table 1). The much reduced grand total variability is again dominated by the first factor, \mathbf{f}'_1 ; however, the f'_{i1} are correlated strongly only with the b_{i3} and, to a lesser extent, b_{i1} . This is quite compatible with the atypically large b_{i3} variability and the water vapor lines in the B_3 and B_1 spectral regions (Figure 2). There are no strong trends in f'_{i1} with the various procedural variables other than perhaps a slight excess variability in the first few spectra of a run (data not shown). This apparent randomness suggests an environmental cause that has a time scale on the order of a single spectral acquisition. We hypothesize that this factor arises from fluctuations in the water vapor content in the beam path between the I_0 and I signal acquisitions.

Figure 4 displays the f'_{i2} (which are very similar to the f_{i3}) as functions of the various procedural variables. Relatively long-term shifts are readily apparent in the Spectra, Filter, and Run time series. A systematic within-run evolution is apparent in the Spectra, Sequence, and

Duplicate series. The first few spectra of most runs give f'_{i2} that are relatively low, approaching equilibrium after six to eight spectra have been acquired. This suggests that factor f'_2 represents both fairly constant among-set environmental differences and changes in environmental conditions within the external sample box during the initial 20 min to 30 min of a given run.

Over at least the range from 5 °C to 50 °C, we show elsewhere that the locations of all seven SRM 2035 and 2065 bands are linear functions of filter temperature [15]

$$b_{ij} = \alpha_j + \beta_j T_i \quad [1]$$

where T_i is the temperature of the i^{th} filter in °C, β_j is the change in band location per °C (slope) for the j^{th} band and α_j is the extrapolated location of the band at zero °C (intercept). The intercepts are known to differ between the two SRMs by up to a few cm^{-1} but the slopes are virtually identical [15]. These independently evaluated slopes are highly correlated with the f_3 loadings (R^2 of 0.971) and very highly correlated with those for f'_2 (R^2 of 0.988).

As discussed in Reference 4, the temperature of the filter can be estimated from the b_{ij} by

$$\hat{T}_i = \frac{\sum_{j=1}^{N_B} w_j \frac{(b_{ij} - \alpha_j)}{\beta_j}}{\sum_{j=1}^{N_B} w_j} \quad [2]$$

where the weights w_j adjust the influence of each band in the calculation. Figure 5 displays the strong linear relationships between the f'_{i2} for the SRM 2035 and 2065 filters and the estimated filter temperatures calculated using w_j that reflect the combined measurement uncertainties (intercept, slope, and band location) of each band. The small offset of about 0.2 °C between the average relationships may reflect small inaccuracies in the estimated temperature coefficient intercepts for one or both SRMs; the relationships for the two materials can be

superimposed by selectively adjusting the intercept values by less than their estimated uncertainties.

PCA of Temperature-Adjusted, SRM-Centered Data. The small offset between the two SRM filters can be eliminated by adjusting the band locations to the average filter temperature rather than to any absolute temperature

$$b'_{ij} = b_{ij} - \beta_j(\hat{T}_i - \bar{T}) \quad [3]$$

and mean-centering the temperature-adjusted values

$$b''_{ij} = b'_{ij} - \bar{b}'_j \quad [4]$$

where \bar{T} and \bar{b}'_j are averages for the SRM 2035 or 2065 data as appropriate.

Table 4 presents summary PCA results for the three most informative PCs for these b''_{ij} data, denoted \mathbf{f}_1'' , \mathbf{f}_2'' , and \mathbf{f}_3'' to distinguish them from the PCs of the previous analyses. As expected given that β_3 is nearly zero and thus the b''_{i3} are little different from the b_{i3} , factor \mathbf{f}_1'' is very similar to \mathbf{f}'_1 . Notably, the correlation between the f''_{i1} and b''_{i1} (0.84) is much stronger than that between the f'_{i1} and b_{i1} (0.49). Given the observed water-vapor lines in the B₁ and B₃ 10% peak-fraction I₀ windows of Figure 2, this “unmasking” of the correlation between the b_{i1} and b_{i3} lends support to the hypothesis of a water vapor-related variance source for these two bands.

Figure 6 displays the standard deviations for each of the bands for the identified sources of variability and for the \mathbf{f}_j'' . In addition to SRM centering (\mathbf{f}_1 to \mathbf{f}'_2), temperature adjustment (\mathbf{f}'_2 to \mathbf{f}_1''), and the water-vapor related \mathbf{f}_1'' variability, \mathbf{f}_2'' and \mathbf{f}_3'' are required to bring all of the band location standard deviations to the expected 0.03 cm^{-1} . In combination, the residual variability represented in \mathbf{f}_4'' through \mathbf{f}_7'' is less than that of \mathbf{f}_3'' and represents an average standard deviation of only 0.026 cm^{-1} .

The \mathbf{f}_2'' loadings are mostly positive and are large for B₂, B₄, B₅, and B₆, a pattern that is plausibly compatible with material heterogeneity. Fifteen of the SRM 2065 filters do provide

consistently high or low f_{i2}'' , the pattern expected for material heterogeneity variability. Further, three of the six filters providing extremely low f_{i1} (Figure 3) are among the 15 filters with consistently extreme f_{i2}'' . This is compatible with material heterogeneity of similar pattern but opposite direction from the known differences between the two SRMs. However, the Spectra and Run time series indicate that the extremely high and low f_{i2}'' tend to occur in within-run clusters – a pattern suggestive of environmental influences.

The f_{i3}'' are modestly correlated with the b_{i5}'' and b_{i6}'' , a pattern plausibly compatible with the HeNe lines observed in the I_0 signals in Figure 2 although the signs of the correlations are opposite. If f_{i3}'' is related to HeNe power fluctuations between the acquisition of the I_0 and I signals, the sign differences might reflect the relative position of the HeNe lines within the two 10% peak-fraction windows: fairly centered for the B_5 window versus the left the edge for B_6 . The extreme high and low f_{i3}'' are fairly uniformly scattered over all the variables, although six of the SRM 2065 filters do provide consistently high or low f_{i3}'' .

PCA of Temperature-Adjusted, SRM-Centered Follow-Up Data. In the absence of model systems for f_{i2}'' and f_{i3}'' , the data of the primary study cannot in themselves resolve whether either or both of these PCs represent material heterogeneity. However, if any of the PCs of the primary study data represent among-filter band location differences then some related variance should be manifest in new spectra. To this end, ten SRM 2065 filters that consistently provided extremely negative or positive f_{i2}'' were selected for further analysis. A similar analysis of filters giving extreme f_{i3}'' was contemplated but proved unnecessary.

Table 5 presents summary PCA results for the three most informative PCs for temperature-adjusted, SRM-centered b_{ij}'' from the follow-up study. These PCs are denoted \mathbf{g}_1'' , \mathbf{g}_2'' , and \mathbf{g}_3'' to distinguish them from the similar PCs of the primary study's data. Table 6

presents the correlations between the loadings for the primary and the follow-up study data. With a between-factor correlation of nearly 1.0, the coefficients for factor g_1'' are very similar to those of f_1'' (Table 4). Perhaps due to the longer purge period before beginning spectral acquisition or differences in ambient humidity, the magnitude of the g_1'' variability is considerably less than that of f_1'' .

The minor PCs g_4'' through g_7'' are also highly correlated to their corresponding PCs in the primary data, f_4'' through f_7'' , and have similar variability magnitudes. This is somewhat surprising, suggesting that the minor PCs may represent systematic rather than random patterns. However, the total variance of these PCs represents an average standard deviation of only 0.032 cm^{-1} .

The f_{i2}'' are not highly correlated with the g_{i2}'' and are only modestly related to the g_{i3}'' . None of the filters that consistently provided extremely negative or positive “heterogeneity” f_{i2}'' yielded consistently extreme values for any of the follow-up study’s PCs. Rather than representing material heterogeneity, f_{i2}'' appears to represent one or more environmental factors that were not present during the follow-up study.

The f_{i3}'' are well correlated with the g_{i2}'' , if not as strongly as for the minor PCs. More tellingly, the g_{i2}'' are strongly correlated only to b_{i5}'' and the g_{i3}'' only to b_{i6}'' . Since B_5 and B_1 are holmium features and B_6 , B_4 , B_3 , and B_2 are samarium features, the relative absence of variability in other bands of these two PCs suggests that the independence of g_2'' and g_3'' does not arise from independent variation of these two constituent rare-earth oxides. If these two bands are influenced by short-term differences in the HeNe line intensities (i.e., between I_0 and I signal acquisition), the independence of the factors must reflect the relative position of the HeNe lines within the 10% peak-fraction windows.

Based upon evaluation of the I_0 signals of the filters with the most extreme f_{i2}'' , we speculate that f_2'' represents short-term fluctuations in the tungsten light source. Figure 7 displays deviations from the average I_0 for four most negative and four most positive spectra. If these spectral differences did not persist throughout signal acquisition, then coordinated shifts in the locations of many of the bands could occur. Given that the shifts are not simple offsets, different sets of bands may show coordinated shifts in different spectra. We currently have no explanation for the non-occurrence of this fluctuation during the follow-up study.

CONCLUSIONS

There is considerable information in the variance/covariance structure of SRM 2065 spectra b_{ij} measurements. Multivariate evaluation enables isolation, identification, and quantification of the major components of variance in these homogeneity data. Sequential removal of the PCs allows calculation of the upper bounds of the material heterogeneity for this SRM batch. PCA also identifies important instrument parameters that should be controlled (or at least understood) when x-axis accuracy is essential. We anticipate that similar evaluation of spectra taken at different times or under different operating parameters will illuminate other aspects of instrument performance.

Figure 6 illustrates this process. The major source of variance is the difference between SRM 2035 and SRM 2065. Although of the same nominal composition, the production of the glass melts used for the two SRMs were separated in time by about 2 years. Small differences in composition or processing history easily account for the small band location differences between the two materials.

The next largest source of band location variance is water vapor. The b_{i3} are strongly influenced by short-term water vapor fluctuations along the beam path. The location of b_{i1} are also influenced but to a much lesser extent. The influence of water on these band locations could be minimized in several ways. Direct engineering solutions, such as improving the purge efficiency and/or using a vacuum system may be economically impractical. In this study, 256 co-adds (112 second scan time) were performed for each filter and air reference measurement. Reducing the time (i.e., fewer co-adds) for both reference (I_0) and signal (I) acquisition as well as reducing the optical pathlength required by the external sample box (currently in excess of 1 m) could reduce the water vapor effects. Deconvolution of the water bands from the air reference and sample single-channel spectra is feasible: at least one commercial FT-IR instrument now uses this approach to reduce water interference in IR spectra [16]. However,

since only one band of this SRM is seriously affected, it may be more judicious for those applications requiring band location long-term precision of better than 0.3 cm^{-1} to simply ignore B_3 for wavenumber/wavelength calibrations.

The temperature of the filter during spectral acquisition is the next major variability source. Knowledge of the relationships between band location and filter temperature enables adjusting the measured data to represent a common filter temperature [4]. Such adjustment reduces the location variability of all bands of all filters to less than 0.04 cm^{-1} and most to below 0.03 cm^{-1} . This reduction is illustrated in Figure 6 as the transition from f_2' to f_1' .

Further reduction of variability in selected bands (especially B_5 and B_6) may be achieved by detailed examination of the individual PCs. PCs f_2'' and f_3'' are tentatively associated with short-term source fluctuation and HeNe plasma lines, respectively. Accounting for these brings the standard deviations for both b_{i5} and b_{i6} to below the 0.03 cm^{-1} system precision; however, experimentally eliminating these sources is likely to be difficult. A beam block designed to eliminate the major reflected HeNe and plasma lines was used throughout this homogeneity study. Complete removal of these lines is difficult without seriously affecting source throughput. Notch filters are a potential solution, if a higher power HeNe were used as the alignment laser. A stabilized source, especially if mounted externally, could remove or reduce the f_2'' variability – and could have the additional advantage of isolating a major cause of instrumental heating.

An upper bound on material heterogeneity effects on band location among the SRM 2065 filters is estimated to be 0.038 cm^{-1} (the s_b'' of Table 4, excluding B_{i3}'') and not the original 0.075 cm^{-1} (the S_{among} of Table 1). If our identification of variances from short-term white light and the HeNe laser are correct, the material heterogeneity bound reduces to less than 0.02 cm^{-1} for all bands within this series of SRM wavelength/wavenumber standards.

DISCLAIMER

Certain commercial materials, instruments, software, and equipment are identified in this paper to specify the experimental procedure as completely as possible. In no case does such identification imply a recommendation or endorsement by the National Institute of Standards and Technology, nor does it imply that the material, instrument, software, or equipment is necessarily the best available for the purpose.

ACKNOWLEDGMENTS

We thank Katherine E. Sharpless for her constructive criticism and patient guidance towards clear(er) language and structure for this and related reports. We thank Pamela Chu for quantitatively modeling band-location interference signals expected from common environmental gases.

REFERENCES

- 1 Standard Reference Material SRM 2035 Near Infrared Transmission Wavelength Standard from 10300 cm^{-1} to 5130 cm^{-1} ; National Institute of Standards and Technology; Gaithersburg, MD, USA, 1999. <http://srmcatalog.nist.gov/>
- 2 S.J. Choquette, J.C. Travis, L.E. O'Neal, C. Zhu, D.L. Duewer, *Spectroscopy* 16 (2000) 14-19.
- 3 Standard Reference Material SRM 2065 UV-Visible, Near-Infrared Transmission Wavelength/Vacuum Wavenumber Standard; National Institute of Standards and Technology; Gaithersburg, MD, USA, 2002. <http://srmcatalog.nist.gov/>
- 4 S.J. Choquette, L.E. O'Neal, D.L. Duewer, L.M. Hannsen, C. Zhu, Preprint available from Authors.
- 5 D.G. Cameron, J.K. Kauppinen, D.J. Moffat, H.H. Mantsch, *Appl. Spectrosc.* 36 (1982) 245-250.
- 6 ASTM E1421-99, Standard Practice for Describing and Measuring Performance of Fourier Transform Mid-Infrared (FT-MIR) Spectrometers Level Zero and Level One Tests, In *Annual Book of ASTM Standards*, ASTM, West Conshohochen PA, USA, 2001; Vol. 03.06. <http://www.astm.org>
- 7 <http://www.chm.bris.ac.uk/org/chemometrics/addins/index.html>
- 8 G. Guelachvili, K.N.Rao, *Handbook of Infrared Standards II*, Academic Press, San Diego, CA USA, 1993.
- 9 V. Kaufman, B. Edlen, *J. Phys. Chem. Ref. Data*, 3 (1974) 825.
- 10 D.C. Hoaglin, F. Mosteller, J.W. Tukey, eds. *Fundamentals of exploratory analysis of variance*, Wiley, New York, NY USA, 1991.
- 11 R.G. Brereton, *Analyst* 120 (1995) 2313-2336.
- 12 E.R. Malinowski, *Factor Analysis in Chemistry, 2nd Ed.*, Wiley, New York, NY USA, 1991.
- 13 I.T. Jolliffe, *Principal Components Analysis*, Springer-Verlag, New York, NY USA, 1986.
- 14 R.G. Brereton, *Analyst* 125 (2000) 2125-2154.
- 15 S.J. Choquette, L.E. O'Neal, D.L. Duewer, *Anal. Chem.* (2003), in press. (Rare-Earth Glass Reference Materials for Near Infrared Spectrometry: Correcting and Exploiting Temperature Dependencies)
- 16 Perkin Elmer, Spectrum-One FT-IR, Shelton, CT.

Table 1. Single-Factor Analysis of Variance of Original b_{ij} , cm^{-1}

Band	SRM 2065 ^a					SRM 2035 ^b		$\Delta_{2065-2035}$ ^g
	Mean	s_{within} ^c	s_{among} ^d	s_{comb} ^e	F ^f	Mean	s_{within} ^c	
B ₁	5139.28	0.025	0.023	0.034	4.89	5138.54	0.028	0.74(4)
B ₂	6806.29	0.026	0.036	0.045	11.95	6804.68	0.053	1.61(7)
B ₃	7314.80	0.197	0.075	0.210	0.87	7313.27	0.326	1.5(4)
B ₄	8180.13	0.027	0.035	0.044	9.67	8178.72	0.042	1.41(6)
B ₅	8682.79	0.033	0.030	0.044	4.85	8681.88	0.035	0.91(6)
B ₆	9294.45	0.036	0.039	0.053	6.92	9293.92	0.059	0.53(8)
B ₇	10245.72	0.014	0.010	0.018	3.05	10245.58	0.018	0.14(3)

- a Nominally six replicate measurements each for 85 SRM 2065 filters
- b 125 replicate measurements of the control filter, SRM 2035 #18
- c Replicate standard deviation
- d Among-filter standard deviation
- e Combined standard deviation, $\sqrt{s_{within}^2 + s_{among}^2}$
- f One-way ANOVA F-ratio (here, $F \cong 6 s_{among}^2 / s_{within}^2$) for the null hypothesis of no among-filter band location differences. The critical F for rejecting this null hypothesis is 1.30.
- g Difference between SRM 2065 and SRM 2035 mean values. The digits in parenthesis denote combined uncertainty in units of the last reported digit of the mean difference.

Table 2. Summary PCA Results for Mean-Centered Original b_{ij}

Band	Loadings ^a			Measurement – Factor Correlations ^b			Standard Deviations ^c , cm^{-1}				s_b ^d cm^{-1}	
	f_1	f_2	f_3	f_1	f_2	f_3	f_1	f_2	f_3	f_{4-7}		
B ₁	0.250	-0.069	0.374	0.99	-0.04	0.09	0.293	0.013	0.027	0.022	0.295	
B ₂	0.543	-0.356	-0.391	0.99	-0.11	-0.04	0.636	0.067	0.028	0.014	0.641	
B ₃	0.537	0.839	-0.008	0.97	0.24	0.00	0.630	0.159	0.001	0.002	0.650	
B ₄	0.476	-0.312	-0.255	0.99	-0.11	-0.03	0.557	0.059	0.018	0.017	0.561	
B ₅	0.307	-0.209	0.433	0.99	-0.11	0.09	0.359	0.039	0.031	0.025	0.364	
B ₆	0.178	-0.151	0.663	0.96	-0.13	0.22	0.208	0.029	0.048	0.022	0.217	
B ₇	0.049	-0.033	-0.125	0.96	-0.10	-0.15	0.058	0.006	0.009	0.013	0.060	
							s_f ^e , cm^{-1}	1.172	0.189	0.072	0.047	1.190 ^f

- a Factor loadings for projecting the (b_{ij} - mean over all spectra) onto the three largest PCs for the 636 spectra.
- b The correlations between the b_{ij} measurements and their f_{ik} factor scores over all 636 spectra.
- c The contribution of the j^{th} band to the variability of the k^{th} factor, in standard deviation form, is (the standard deviation of the f_{ik})(absolute value of the f_k loading for B_j).
- d The total standard deviation of the j^{th} band.
- e The total standard deviation of the k^{th} factor.
- f The grand total standard deviation for all bands or PCs.

Table 3. Summary PCA Results for SRM-Centered b_{ij}

Band	Loadings ^a			Measurement – Factor Correlations ^b			Standard Deviations ^c , cm^{-1}				s'_b ^d cm^{-1}	
	f'_1	f'_2	f'_3	f'_1	f'_2	f'_3	f'_1	f'_2	f'_3	f'_{4-7}		
B ₁	0.068	0.333	-0.163	0.49	0.79	-0.23	0.015	0.025	0.007	0.009	0.031	
B ₂	0.015	-0.546	0.290	0.08	-0.90	0.29	0.003	0.041	0.013	0.014	0.045	
B ₃	0.997	0.011	0.016	1.00	0.00	0.00	0.225	0.001	0.001	0.001	0.225	
B ₄	0.017	-0.419	0.566	0.09	-0.73	0.60	0.004	0.031	0.026	0.013	0.042	
B ₅	-0.004	0.301	0.481	-0.02	0.55	0.53	0.001	0.022	0.022	0.026	0.041	
B ₆	-0.031	0.551	0.575	-0.13	0.78	0.50	0.007	0.041	0.026	0.019	0.052	
B ₇	0.004	-0.142	0.084	0.05	-0.63	0.23	0.001	0.011	0.004	0.013	0.017	
							s'_f ^e , cm^{-1}	0.226	0.074	0.045	0.041	0.245 ^f

- a Factor loadings for projecting the b'_{ij} (b_{ij} - mean over SRM 2035 or SRM 2065 spectra) onto the three largest PCs for the 636 spectra.
- b The correlations between the b'_{ij} and their f'_{ik} PCs over all 636 spectra.
- c The contribution of the j^{th} band to the variability of the k^{th} factor, in standard deviation form, is the (standard deviation of the f'_{ik})(absolute value of the f'_k loading for B_j).
- d The total standard deviation of the j^{th} band.
- e The total standard deviation of the k^{th} factor.
- f The grand total standard deviation for all bands or PCs.

Table 4. Summary PCA Results for Temperature-Corrected, SRM-Centered b_{ij}''

Band	Loadings ^a			Measurement – Factor Correlations ^b			Standard Deviations ^c , cm^{-1}				s_b'' ^d cm^{-1}	
	f_1''	f_2''	f_3''	f_1''	f_2''	f_3''	f_1''	f_2''	f_3''	f_{4-7}''		
B ₁	0.069	-0.066	0.017	0.84	-0.16	0.03	0.016	0.003	0.001	0.010	0.019	
B ₂	0.013	0.132	-0.085	0.22	0.47	-0.21	0.003	0.006	0.003	0.011	0.013	
B ₃	0.997	0.019	-0.013	1.00	0.00	0.00	0.225	0.001	0.000	0.001	0.225	
B ₄	0.015	0.427	-0.060	0.13	0.77	-0.08	0.003	0.020	0.002	0.016	0.026	
B ₅	-0.003	0.551	0.808	-0.02	0.70	0.71	0.001	0.026	0.026	0.004	0.037	
B ₆	-0.029	0.700	-0.577	-0.17	0.85	-0.48	0.007	0.033	0.018	0.005	0.038	
B ₇	0.003	0.043	-0.061	0.05	0.16	-0.15	0.001	0.002	0.002	0.012	0.013	
							s_f'' ^e , cm^{-1}	0.226	0.047	0.032	0.026	0.234 ^f

- a Factor loadings for projecting the b_{ij}'' (temperature adjusted b_{ij} - mean over temperature-adjusted SRM 2035 or SRM 2065 spectra) onto the three largest PCs for the 636 spectra.
- b The correlations between the b_{ij}'' and their f_{ik}'' factor scores over all 636 spectra.
- c The variance contribution of the j^{th} band to the k^{th} factor, in standard deviation form, is the (standard deviation of the f_{ik}'')(absolute value of the f_k'' loading for B_j).
- d The total standard deviation of the j^{th} band.
- e The total standard deviation of the k^{th} factor.
- f The total standard deviation for all bands or PCs.

Table 5. Summary PCA Results for Temperature-Corrected, SRM-Centered b''_{ij} Follow-Up Data

Band	Loadings ^a			Measurement – Factor Correlations ^b			Standard Deviations ^c , cm^{-1}				s''_b ^d cm^{-1}	
	g''_1	g''_2	g''_3	g''_1	g''_2	g''_3	g''_1	g''_2	g''_3	g''_{4-7}		
B ₁	0.065	0.001	-0.079	0.53	0.00	-0.22	0.009	0.000	0.004	0.013	0.016	
B ₂	0.010	0.105	0.240	0.07	0.42	0.58	0.001	0.008	0.011	0.013	0.018	
B ₃	0.997	0.014	-0.004	1.00	0.01	0.00	0.132	0.001	0.000	0.001	0.132	
B ₄	0.032	-0.028	0.238	0.18	-0.09	0.45	0.004	0.002	0.011	0.021	0.024	
B ₅	-0.014	0.989	0.076	-0.03	1.00	0.05	0.002	0.073	0.003	0.002	0.073	
B ₆	0.000	-0.100	0.935	0.00	-0.17	0.98	0.000	0.007	0.042	0.003	0.043	
B ₇	0.020	-0.014	0.013	0.15	-0.06	0.03	0.003	0.001	0.001	0.017	0.017	
							s''_f ^e , cm^{-1}	0.132	0.074	0.045	0.033	0.161 ^f

- a Factor loadings for projecting the follow-up data b''_{ij} (temperature adjusted b_{ij} - mean over temperature-adjusted SRM 2035 or SRM 2065 spectra) onto the three largest PCs for the 185 spectra.
- b The correlations between the follow-up data b''_{ij} and their g''_{ik} factor scores over all 185 spectra.
- c The contribution of the j^{th} band to the variability of the k^{th} factor, in standard deviation form, is the (standard deviation of the g''_{ik})(absolute value of the g''_k loading for B_j).
- d The total standard deviation of the j^{th} band.
- e The total standard deviation of the k^{th} factor.
- f The grand total standard deviation for all bands or PCs.

Table 6. Correlations Among Original and Follow-up Loadings

	$\mathbf{g''_1}$	$\mathbf{g''_2}$	$\mathbf{g''_3}$	$\mathbf{g''_4}$	$\mathbf{g''_5}$	$\mathbf{g''_6}$	$\mathbf{g''_7}$
$\mathbf{f''_1}$	1.00	-0.15	-0.31	-0.06	-0.05	-0.35	-0.08
$\mathbf{f''_2}$	-0.40	0.34	0.76	0.27	-0.15	-0.59	-0.18
$\mathbf{f''_3}$	-0.04	0.91	-0.62	0.09	-0.06	-0.04	-0.01
$\mathbf{f''_4}$	0.05	-0.21	-0.16	0.95	-0.20	0.12	-0.01
$\mathbf{f''_5}$	-0.04	-0.01	-0.11	0.21	0.97	-0.07	0.00
$\mathbf{f''_6}$	-0.31	-0.28	-0.52	-0.14	-0.07	0.99	-0.08
$\mathbf{f''_7}$	-0.07	-0.06	-0.10	0.00	-0.04	-0.17	1.00

FIGURE CAPTIONS

- Figure 1. Representative NIR Absorbance Spectrum of SRM 2065 and its Dry Nitrogen Purge Gas Reference I_0 .
- Figure 2. 10%-Fraction Spectral Windows. The dark lines of the lower graphical segment present the 10%-fraction spectral windows for the seven NIR absorption features of interest. These data are used to calculate each b_{ij} . The number beneath each peak is the number of data used in the b_{ij} calculations (4 cm^{-1} resolution spectra, 0.97 cm^{-1} x-axis spacing). The light lines of the upper segment represent the variability in the purge-gas reference I_0 spectra within the spectral windows. The text above the variability structure in five of the seven windows identifies the location of known H_2O vapor absorption and HeNe emission lines.
- Figure 3. f_1 Scores vs Procedural Variables. The top segment (Spectra) displays the f_{11} as a function of spectrum index, 1 through 636. The “+” denote values of middle magnitude (the central 50%, those between the first and third quartiles); the solid circles denote low magnitude values (the smallest 25%); and the open circles denote high magnitude values (the largest 25%). The f_{11} have been normalized (z-scored) to have unit standard deviation with all values less than -3 and greater than +3 displayed at the respective graphical margins. The remaining segments display the same 636 data as functions of: (1) filter wheel position (Position), 0 through 5. (2) order of initial measurement for a given filter (Filter), 0 through 85, with all 125 control filter values plotted at 0 and all 12 spectra for filter 206 plotted at 1. (3) run index (Run), 1 through 18. (4) spectrum-of-run (Sequence) order, 1 through 37. (5) replication-of-run (Duplicate), 1 through 7. The vertical lines in the Spectra segment denote the beginning of each of the 18 Runs, with the longer lines denoting the beginning of each of the 9 days needed to acquire all spectra. The “x” along the

zero-line of the Filter segment denote filters with replicate spectra that consistently have high or low magnitude f_{i1} values.

Figure 4. f'_2 Scores vs Procedural Variables. See Figure 3 for legend.

Figure 5. f'_2 Scores vs Certainty-weight Calculated Filter Temperature. The open circles and dashed summary line denote SRM 2035 data; the solid circles and solid summary line denote SRM 2065 data.

Figure 6. Standard Deviation Attributable to Each of the PCs. The digits 1 through 7 connected with solid lines denote the magnitude of the variability (as a standard deviation, cm^{-1}) of each band to the named PCs. The dashed line at 0.03 cm^{-1} represents the spectrophotometer's expected long-term precision.

Figure 7. I_0 Differences among Spectra with Extreme f'_{i2} Spectral Values. The light lines denote I_0 spectral differences (relative to the "representative" I_0 spectrum in Fig. 1) for four spectra with extremely positive f'_{i2} . The dark lines denote four spectra with extremely negative f'_{i2} .

Figure 1

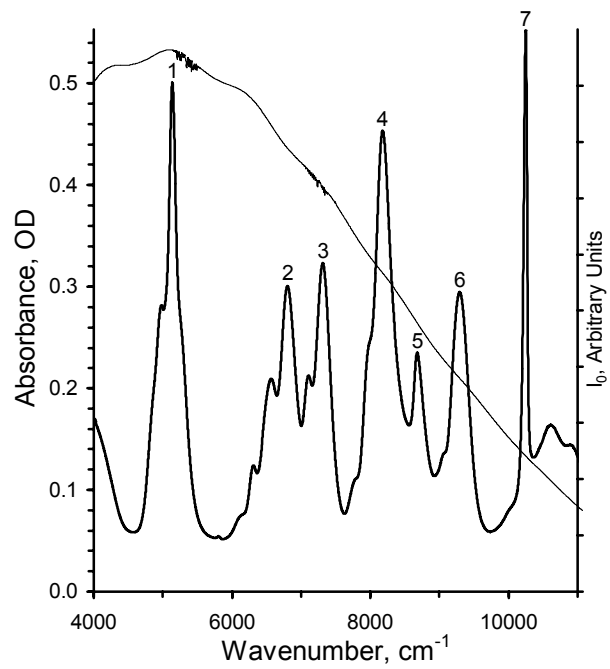


Figure 2

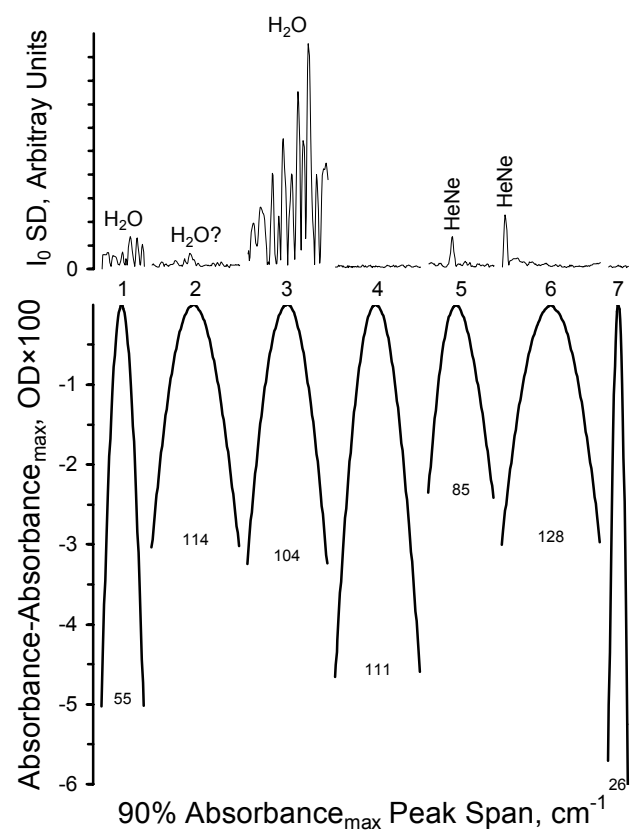


Figure 3

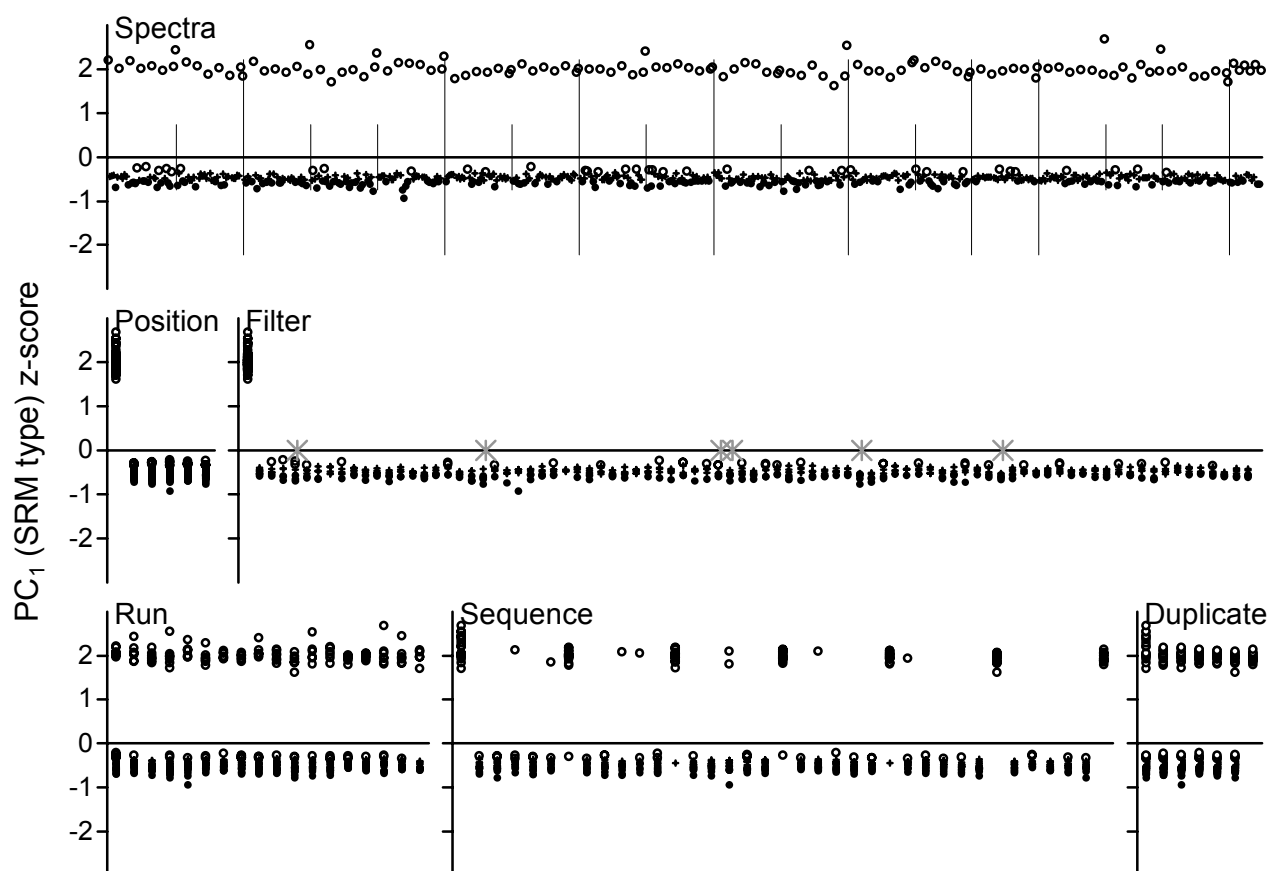


Figure 4

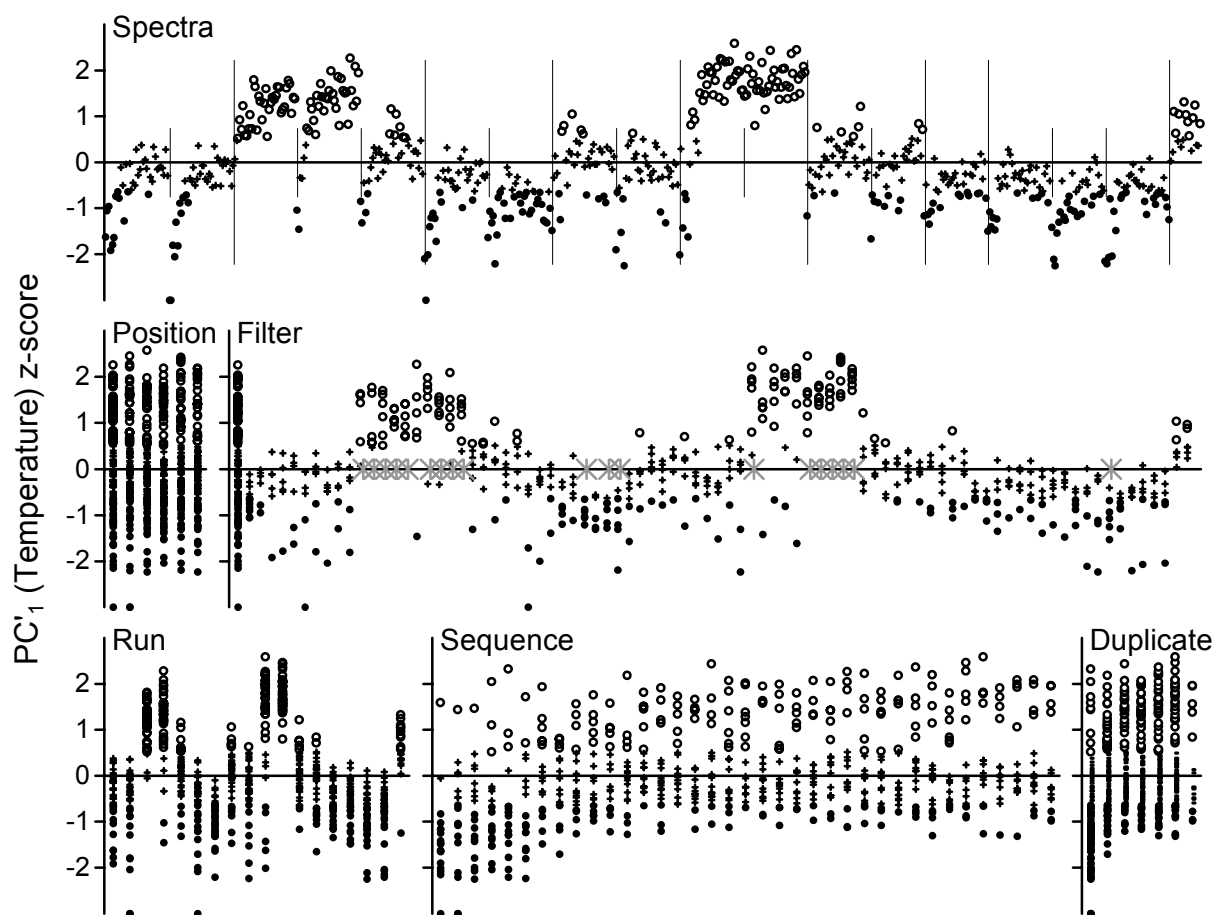


Figure 5

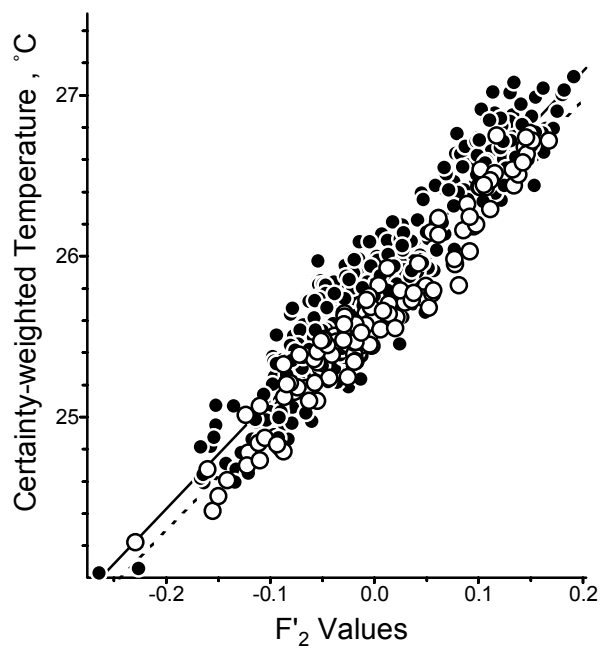


Figure 6

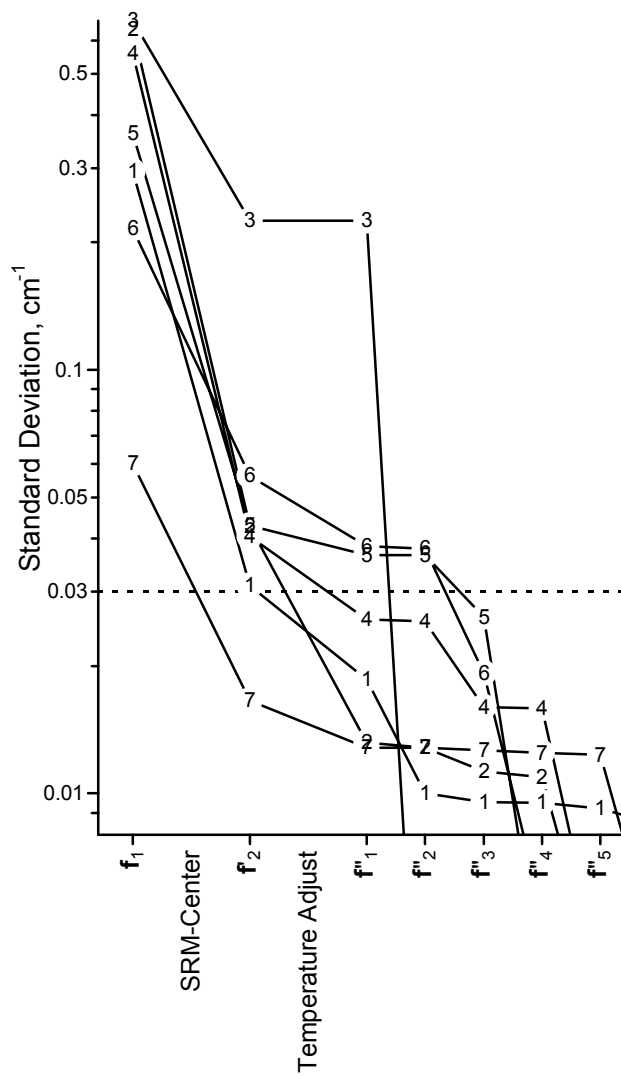


Figure 7

